Supplementary Information

Single-Iron, Cobalt, Nickel and Copper-Atom Catalysts for Selective Reduction of Oxygen to H_2O_2

Cuizhu Ye, [a,b] *Yongfang Zhou,* [a,b] *Hongying Li* [d] *and Yi Shen* [*a,b,c]

[a]School of Food Science and Engineering, South China University of Technology, Guangzhou 510640, China

[b]China-Singapore International Joint Research Institute, Guangzhou Knowledge City, Guangzhou 510663, China

[c]Overseas Expertise Introduction Center for Discipline Innovation of Food Nutrition and Human Health (111 Center), Guangzhou, 510640, China

[d]Institute of High-Performance Computing, Agency for Science, Technology and Research, 138632, Singapore.

[*]Corresponding author, Email: feyshen@scut.edu.cn

List of Contents:

Experimental section

Chemicals

Anhydrous ethanol was purchased from the Nanjing Chemical Reagent Co., Ltd. (Nanjing, China). Isopropyl alcohol was purchased from Tianjin Fuyu Fine Chemical Co., Ltd. Hydrochloric acid, sulfuric acid, nitric acid and hydrogen peroxide 30% were provided by Guangdong chemical factory. Sodium dodecyl benzene sulfonate (SDBS, $C_{18}H_{29}NaO_3S$) was purchased from the Shanghai Lingfeng Chemical Reagent Co., Ltd.

Nickel nitrate was purchased from the Tianjin Damao Chemical Reagent Factory (Tianjin, China). Cupric nitrate trihydrate was purchased from Saen Chemical technology Co., Ltd. Iron nitrate nonahydrate, cobalt nitrate hexahydrate, furfural (99%), cyanamide (50% aqueous solution containing 0.25% methyl formate stabilizer), were purchased from Shanghai Aladdin Biochemical Technology Co., Ltd. Titanic sulfate ($Ti(SO_4)_2$, ≥96%), potassium hydroxide (99.99% electronic grade) and copper nanoparticles (Cu NPs, 99.9% metals basis) were purchased from Shanghai Macklin Biochemical Co., Ltd. Nitrogen and oxygen (purity > 99.99%) were purchased from the Guangzhou Yuejia Gas Co., Ltd. (Guangzhou, China). Nafion solution (20%) was purchased from the Chemours Company FC, LLC. The 18.25 MΩ/cm deionized water was produced by an ultra-pure water system (WP-UP-YJ-40, Sichuan, China).

Characterization

A transmission electron microscope (TEM, FEI Tecnai F30) was used to observe the morphology of the samples. High-angle annular dark field scanning transmission electron microscopy (HAADF-STEM) was conducted on an alternative microscope (ARM200F JEOL). The metal content in the catalyst was quantified by inductively coupled plasma - optical emission spectrometer (ICP-OES). The crystal structures of the catalysts were revealed by X-ray diffraction (XRD, D8 advance, polycrystalline powder diffraction). Raman spectra was recorded on Renishaw InVia Raman spectrometer with the laser source 532 nm. The Brunauer–Emmett–Teller (BET) surface area and pore size distribution of samples were determined by TriStar II 3020.

Table S1 Metal contents in the samples as determined by ICP-AES

Sample	Metal content by ICP (wt. %)
Fe/NCNSs	0.31
Co/NCNSs	0.24
Ni/NCNSs	0.26
Cu/NCNSs	0.34

Table S2 Onset potentials of the catalysts in 0.1 M KOH, $HClO_4$ and PBS solutions

Samples	Disk electrode			Ring electrode		
	KOH	$HClO_4$	PBS	KOH	$HClO_4$	PBS
Fe/NCNSs	0.72	0.70	0.70	0.69	0.77	0.73
Co/NCNSs	0.74	0.76	0.75	0.68	0.71	0.77
Ni/NCNSs	0.77	0.69	0.75	0.77	0.68	0.75
Cu/NCNSs	0.75	0.76	0.76	0.76	0.82	0.77
NCNSs	0.74	0.75	0.72	0.70	0.80	0.72
CuNPs	0.65	0.29	0.31	0.66	0.025	0.12
GCE	0.63	0.69	0.48	0.72	0.50	0.55

Table S3 Summary of the performance of the electrocatalysts for H_2O_2 production in alkaline media

Catalyst	Catalyst loading (μg/cm^2)	J_L or $J_{0.1\ V}$ (Disk, mA cm^{-2})	J_L or $J_{0.1\ V}$ (Ring, mA cm^{-2})	H_2O_2%	Potential	Productivity (mol/g/L/h)	Stability test	Reference
Cu/NCNSs	100	2.5 (0.53 mA)	2.15 (0.45 mA)	96 ~ 100%	0.1 ~ 0.6 V	5.1 (204 mmol/g/h)	20 h	This work
Mo_2CT_x:Fe	250	~1.7	~1.4	67 ~ 100%	0.2 ~ 0.7 V	NA	4 h	J. Am. Chem. Soc. 2021, 143, 5771−5778[1]
CuO_x/G-30	NA	~1.6	NA	76 ~ 84%	0.4 ~ 0.7 V	NA	~8.3 h	Chem. Commun., 2021, 57, 4118[2]
MCHS-9:1	100	3.0	0.8	56%	0.4 ~ 0.8 V	NA	2500 cycles	ACS Catal. 2020, 10, 7434−7442[3]
Co-N-C	100	3.8	0.13 mA	60 ~ 70%	0.1 ~ 0.5 V	193.1 mmol/g/h	3 h	J. Am. Chem. Soc. 2019, 141, 12372−12381[4]
FA-15TRZ	232	NA	NA	NA		0.5 mmol/g/h	NA	Catal. Today 2020, 356, 132–140[5]
Ni MOF NSs-6	NA	0.65 mA	0.175 mA	~ 98%	0.2 ~ 0.6 V	80 mmol/g/h	20000 cycles	Angew. Chem. Int. Ed. 2021, 60, 11190–11195[6]
Mo_1/OSG-H	100	2.78	0.2 mA	95%	0.35 ~ 0.75 V	NA	8 h	Angew. Chem. Int. Ed. 2020, 59, 9171–9176[7]
Co–POC–O	100	~ 0.57 mA	~ 0.35 mA	~ 85.6%	0.5 ~ 0.8 V	813 mg L^{-1} h^{-1}	10 h	Adv. Mater. 2019, 31, 1808173[8]
Fe-N-C	100	4	NA	32%	0.1 ~ 0.8 V	NA	1000 cycles	Angew. Chem. Int. Ed. 2017, 56, 8809 – 8812[9]
S-MC-1	255	2.373	0.065 mA	70 ~ 80%	-0.3 ~ 0.4 V	NA	NA	Carbon 2015, 95, 949-963[10]
MesoC	510	4	2	60 ~80%	0.2 ~ 0.7 V	NA	11000 cycles	ACS Sustainable Chem. Eng. 2018, 6, 311−317[11]
Printex B	810	0.3 mA	0.010 mA	82 ~ 92%	0.1 ~ 1.0 V	NA	NA	Electrocatalysis 2016, 7, 60–69[12]

O-CNTs	200	0.54 mA	0.41 mA	~ 90%	0.4 ~ 0.7 V	NA	NA	Nat. Catal. 2018, 1, 156–162 [13]
CNTs	200	0.35 mA	0.14 mA	~ 60%	0.4 ~ 0.7 V	NA	NA	Nat. Catal. 2018, 1, 156–162 [13]
BN-C1	510	3.5	2.1	60 ~ 90%	0.2 ~ 0.8 V	NA	50 h	J. Am. Chem. Soc. 2018, 140, 7851−7859[14]
Urea-C_3N_4	NA	0.4 mA	0.1 mA	88 ~ 90 %	0.1 ~ 0.6 V	56.3	~ 24 h	Adv. Mater. Interfaces 2022, 9, 2201325[15]
6h-Pd/TiC	100	~ 2.3	~ 1.7	82 ~ 90%	0.1 ~ 0.7 V	594 mg L^{-1} h^{-1}	10 h	J. Am. Chem. Soc. 2022, 144, 2255−2263[16]
In SAs/NSBC	100	0.7 mA	0.208 mA	~ 95%	0.4 ~ 0.7 V	6.49 mol/g/h By PEMFC	12 h	Angew. Chem. Int. Ed. 2022, 61, e202117347[17]
COF-366-Co	350	2.5	0.8	< 91%	0.3 V	909 mmol/g/h on GDE	3 h	J. Am. Chem. Soc. 2020, 142, 21861−21871[18]

Note: J_L is the limited current density. NA, this data is not available.

Table S4 Summary of the performance of the electrocatalysts for H_2O_2 production in acidic media

Catalyst	Catalyst loading(μg/cm^2)	Onset potential(V)	J_L or $J_{-0.2V}$ (Disk, mA cm^{-2})	J_L or $J_{-0.2V}$ (Ring, mA cm^{-2})	H_2O_2%	Productivity (mol/g/L/h)	Stability test	electrolyte	Reference
Cu/NCNSs	102	0.76	2.0 (0.39 mA)	0.9 (0.18 mA)	70 ~ 81	3.2	20 h	0.1 M $HClO_4$	This work
GO-250	NA	0	NA	0.33	> 62.5	NA	2 h	0.1 M Na_2SO_4 and H_2SO_4 (pH 3)	ChemSusChem 2016, 9, 1194 – 1199[19]
S-MC	255	~ 0.3	0.45 mA	0.07 mA	> 68	NA	NA	0.5 M H_2SO_4	Carbon 2015, 95, 949e963[10]
Co-N-C	100	0.83	2.97 (at 0.1 V)	0.18 mA (at 0.1 V)	< 80	90.9 mmol/g/h	6 h	0.5 M H_2SO_4	J. Am. Chem. Soc. 2019, 141, 12372−12381[4]
Pt-Hg/C	23	NA	3.0	~ 0.6	65 ~ 90	NA	8000 cycles	0.1 M $HClO_4$	Nat. Mater. 2013, 12, 1137-1143[20]
O-CNTs	200	0.28	0.44 mA	0.15 mA	~ 50	NA	NA	0.1 M $HClO_4$	Nat. Catal. 2018, 1, 156–162 [13]
$MoTe_2$	10	0.56	2.25	0.13 mA	< 93	NA	~12 h	0.5 M H_2SO_4	National Science Review 2020, 7, 1360–1366 [21]
Co_1-NG(O)	1000	0.7	2.1	0.9	40 ~ 50	NA	NA	0.1 M $HClO_4$	Nat. Mater. 2020, 19, 436-442[22]

Note: NA, this data is not available.

Table S5 Summary of the performance of the electrocatalysts for H_2O_2 production in neutral media

Catalyst	Catalyst loading(μg/cm^2)	Onset potential(V)	J_L or $J_{-0.2V}$ (Disk, mA cm^{-2})	J_L or $J_{-0.2V}$ (Ring, mA cm^{-2})	H_2O_2%	Productivity (mol/g/L/h)	Stability test	electrolyte	Reference
Cu/NCNSs	102	0.76	1.64 (0.32 mA)	0.89 (0.18 mA)	70 ~ 81	2.2 (86.4 mmol/g/h)	20 h	0.1 M PBS	This work
MNC-600	NA	0.71	1.4	0.09 mA	30 ~ 85.4	9.6 mmol/g/h	NA	0.1 M K_2HCO_3	ChemElectroChem 2022, 9, e202101336[23]
Co-TPP	NA	~ 0.8	1.0	0.1	43 ~ 79	NA	NA	0.1 M PBS	Angew. Chem. Int. Ed. 2020, 59, 4902 –4907[24]
MicroC	510	0.5	3	~ 1.0	40 ~ 80	NA	NA	0.1 M PBS	ACS Sustainable Chem. Eng. 2018, 6, 311−317[11]
Co_1-NG(O)	10	~ 0.7	2.6	1.25	60 ~ 70	NA	NA	0.1 M PBS	Nat. Mater. 2020, 19, 436-442[22]
Mo_1/OSG-H	100	~ 0.6	3	0.13	77	NA	NA	pH 8.7	Angew. Chem. Int. Ed. 2020, 59, 9171–917[7]
Co-N-C	100	~ 0.6	3.8	0.13	55	89.8	NA	0.1 M K_2SO_4	J. Am. Chem. Soc. 2019, 141, 12372−12381[4]
Pd_x-NC	162	~ 0.7	3.3	0.35	> 30	NA	NA	0.1 M PBS	ACS Catal. 2022, 12, 4156−4164[25]

Table S6 J_k values of the samples at different potentials in 0.1 M KOH, $HClO_4$ and PBS solutions

Samples	KOH					$HClO_4$						PBS					
	0.1 V	0.2 V	0.3 V	0.4 V	0.5 V	-0.2 V	-0.1 V	0 V	0.1V	0.2 V	0.3 V	-0.2 V	-0.1 V	0 V	0.1 V	0.2 V	0.3 V
Fe/NCNSs	7.1	4.9	3.1	1.9	1.0	1.08	0.56	0.34	0.24	0.19	0.16	2.47	2.25	1.91	1.30	0.72	0.38
Co/NCNSs	9.4	6.0	3.5	1.9	1.0	2.64	1.74	1.17	0.85	0.66	0.50	-	2.69	2.32	1.76	1.15	0.70
Ni/NCNSs	8.3	6.0	4.3	3.1	2.1	3.03	2.06	1.27	0.80	0.49	0.29	2.90	2.63	2.31	1.83	1.26	0.76
Cu/NCNSs	18.2	11.6	7.1	4.3	2.3	4.09	2.66	1.39	0.75	0.52	0.38	2.87	2.68	2.37	1.82	1.22	0.75
NCNSs	5.0	3.8	2.7	1.6	0.9	2.17	1.40	0.95	0.71	0.53	0.38	2.81	2.57	2.23	1.63	0.98	0.54

Table S7 Selectivity, J_k, *w* and M values of the catalysts in acidic, neutral and alkaline media at 1600 rpm on RRDE

Catalysts		H_2O_2 selectivity (%)			J_k			n			*w* (%)	M
		KOH	$HClO_4$	PBS	KOH	$HClO_4$	PBS	KOH	$HClO_4$	PBS		
Fe/NCNSs	0.1 V	83.1	80	76.4	7.1	0.24	1.30	2.34	2.40	2.39	0.31	56.0
	0.2 V	86.6	78.9	78.8	4.9	0.19	0.72	2.27	2.42	2.30		
	0.3 V	90.2	76.6	80.3	3.1	0.16	0.38	2.19	2.47	2.19		
	0.4 V	91.3	75.2	81.9	1.9	-	-	2.17	2.50	2.02		
	0.5 V	92.9	71.6	81.6	1.0	-	-	2.14	2.57	1.86		
Co/NCNSs	0.1 V	88.4	43.7	67.0	9.4	0.85	1.76	2.23	3.12	2.55	0.24	58.9
	0.2 V	90.0	43.6	69.2	6.0	0.66	1.15	2.20	3.12	2.47		
	0.3 V	91.3	43.8	69.9	3.5	0.50	0.70	2.17	3.12	2.40		
	0.4 V	91.4	44.8	67.5	1.9	-	-	2.17	3.10	2.35		
	0.5 V	91.4	46.1	65.9	1.0	-	-	2.17	3.08	2.26		
Ni/NCNSs	0.1 V	80.1	42.6	66.9	8.3	0.80	1.83	2.40	3.14	2.59	0.26	58.7
	0.2 V	85.8	48.7	68.2	6.0	0.49	1.26	2.28	3.03	2.54		
	0.3 V	88.3	56.5	70.2	4.3	0.29	0.76	2.23	2.87	2.47		
	0.4 V	88.7	61.3	76.5	3.1	-	-	2.23	2.77	2.25		
	0.5 V	91.4	55.8	82.0	2.1	-	-	2.17	2.88	1.92		
Cu/NCNSs	0.1 V	95.6	80.9	75.8	18.2	0.75	1.82	2.09	2.38	2.48	0.34	63.5
	0.2 V	97.7	78.5	76.5	11.6	0.52	1.22	2.05	2.43	2.47		
	0.3 V	98.6	76.7	77.7	7.1	0.38	0.75	2.03	2.47	2.45		
	0.4 V	98.7	75.5	78.2	4.3	-	-	2.03	2.49	2.44		
	0.5 V	99.7	67.2	82.6	2.3	-	-	2.00	2.65	2.36		

Table S8 TOF values of the samples in 0.1 M KOH, $HClO_4$ and PBS solutions

Samples	KOH					$HClO_4$			PBS		
	0.1 V	0.2 V	0.3 V	0.4 V	0.5 V	0.1 V	0.2 V	0.3 V	0.1 V	0.2 V	0.3 V
Fe/NCNSs	4.6	3.4	2.3	1.5	0.8	0.15	0.11	0.09	0.76	0.45	0.25
Co/NCNSs	9.3	6.1	3.7	2.0	1.0	0.29	0.23	0.17	1.15	0.80	0.51
Ni/NCNSs	6.3	5.2	3.9	2.8	2.0	0.25	0.18	0.13	1.08	0.77	0.49
Cu/NCNSs	15.8	10.5	6.5	4.0	2.2	0.48	0.32	0.22	1.06	0.72	0.45

Table S9 H_2O_2 yield rates at 0, 0.2 and 0.3 V in 0.1 M KOH solutions

Potentials	Production in KOH (mol g^{-1} $L^{-1}h^{-1}$)	
	6 h	average
0 V	21.5	3.5
0.2 V	27.2	4.5
0.3 V	24.6	4.1

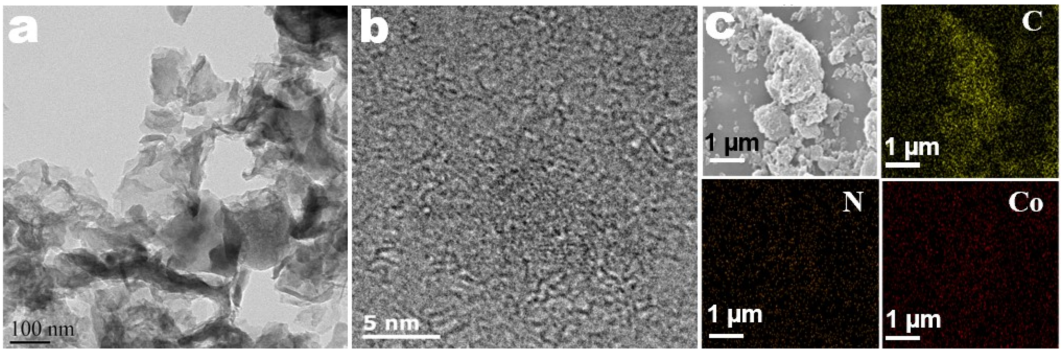

Figure S1 Structural characterization of Co single atoms catalysts. TEM image (a), high-resolution TEM image (b), SEM image and the corresponding elemental mapping images of carbon, nitrogen and cobalt (c) of the Co/NCNSs.

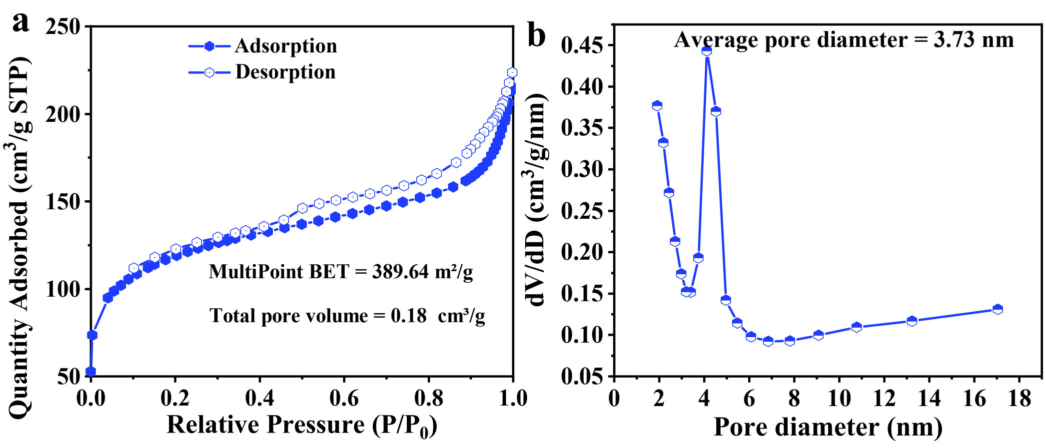

Figure S2 N_2 adsorption-desorption isotherm of the Fe/NCNSs (a) and corresponding pore size distribution (b).

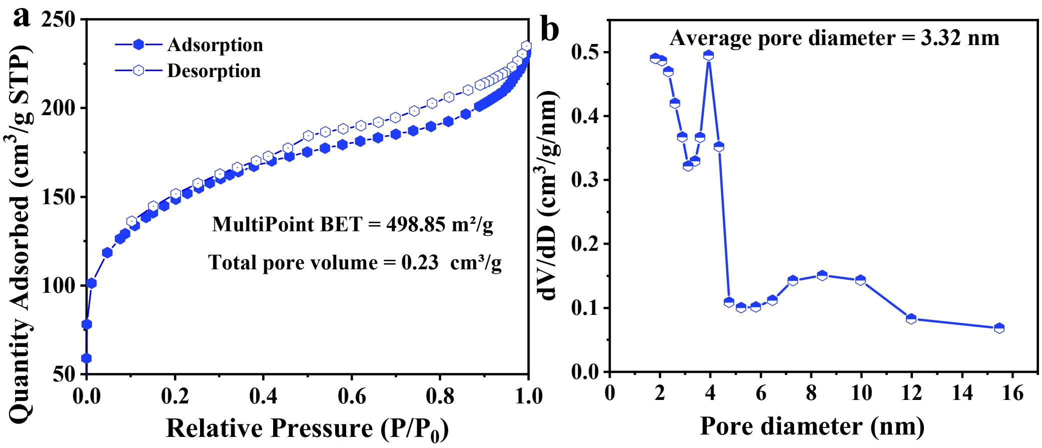

Figure S3 N_2 adsorption-desorption isotherm of the Co/NCNSs (a) and corresponding pore size distribution (b).

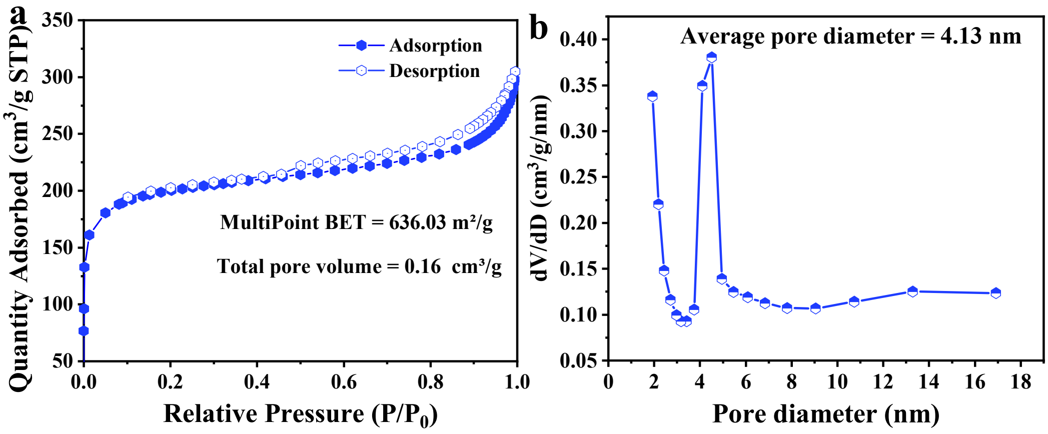

Figure S4 N_2 adsorption-desorption isotherm of the Ni/NCNSs (a) and corresponding pore size distribution (b).

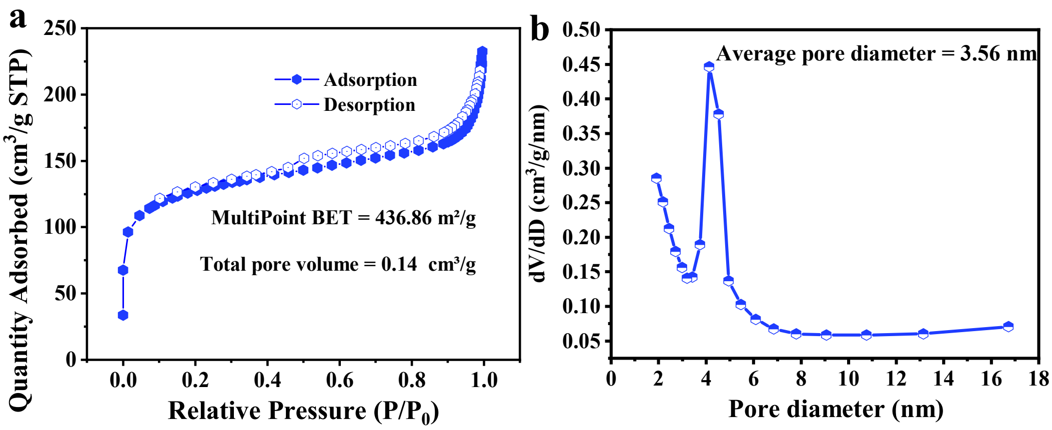

Figure S5 N_2 adsorption-desorption isotherm of the Cu/NCNSs (a) and corresponding pore size distribution (b).

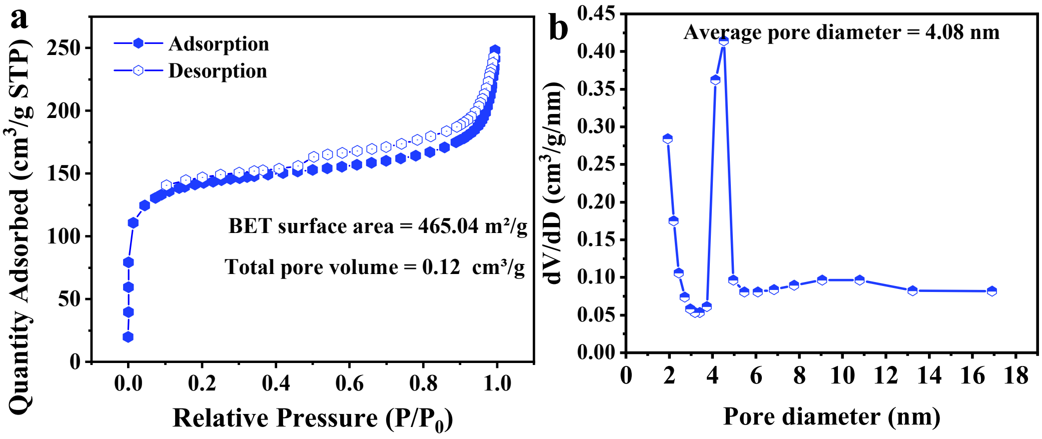

Figure S6 N_2 adsorption-desorption isotherm of the NCNSs (a) and corresponding pore size distribution (b).

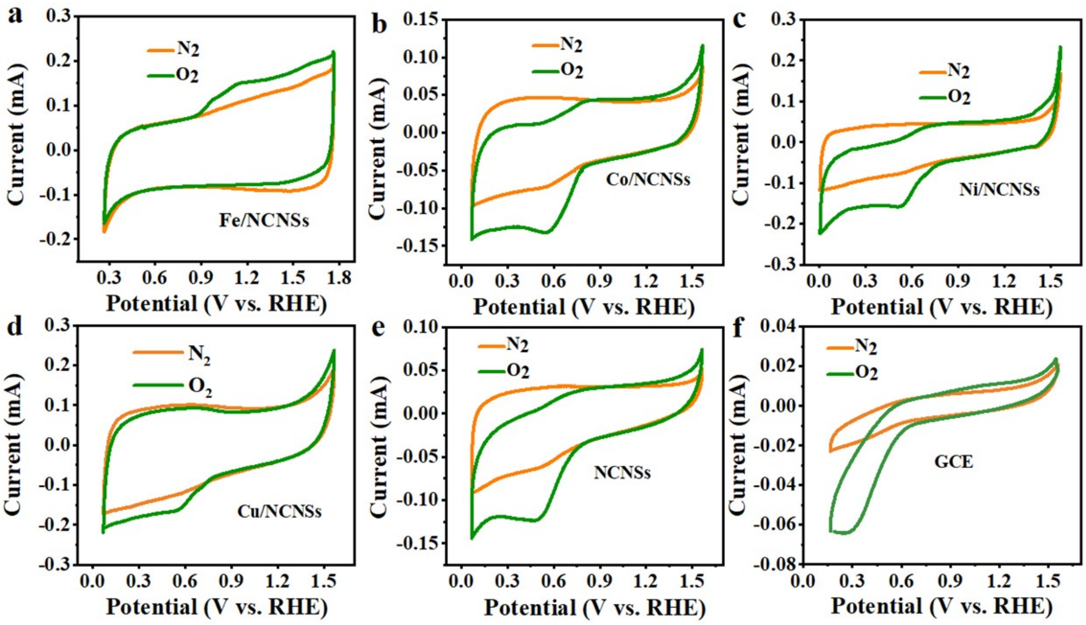

Figure S7 Cyclic voltammetry curves of (a) Fe/NCNSs, (b) Co/NCNSs, (c) Ni/NCNSs, (d) Cu/NCNSs, (e) NCNSs and (f) blank GCE acquired in O_2-saturated and N_2-saturated 0.1 M KOH at a scan rate of 50 mV s^{-1}.

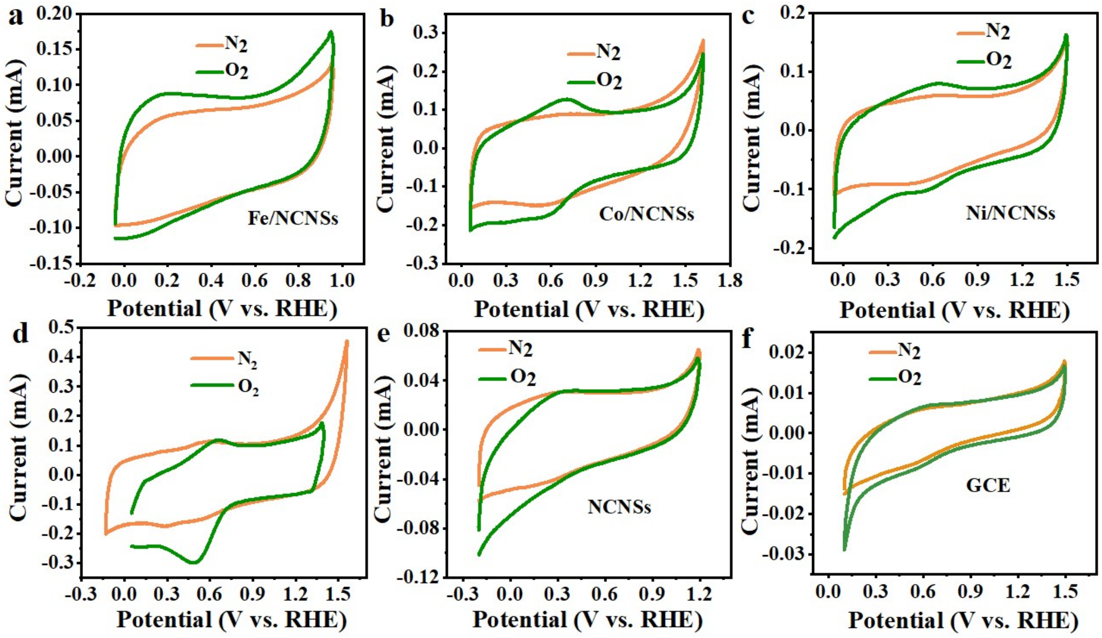

Figure S8 Cyclic voltammetry curves of (a) Fe/NCNSs, (b) Co/NCNSs, (c) Ni/NCNSs, (d) Cu/NCNSs, (e) NCNSs and (f) blank GCE acquired in O_2-saturated and N_2-saturated 0.1 M $HClO_4$ at a scan rate of 50 mV s^{-1}.

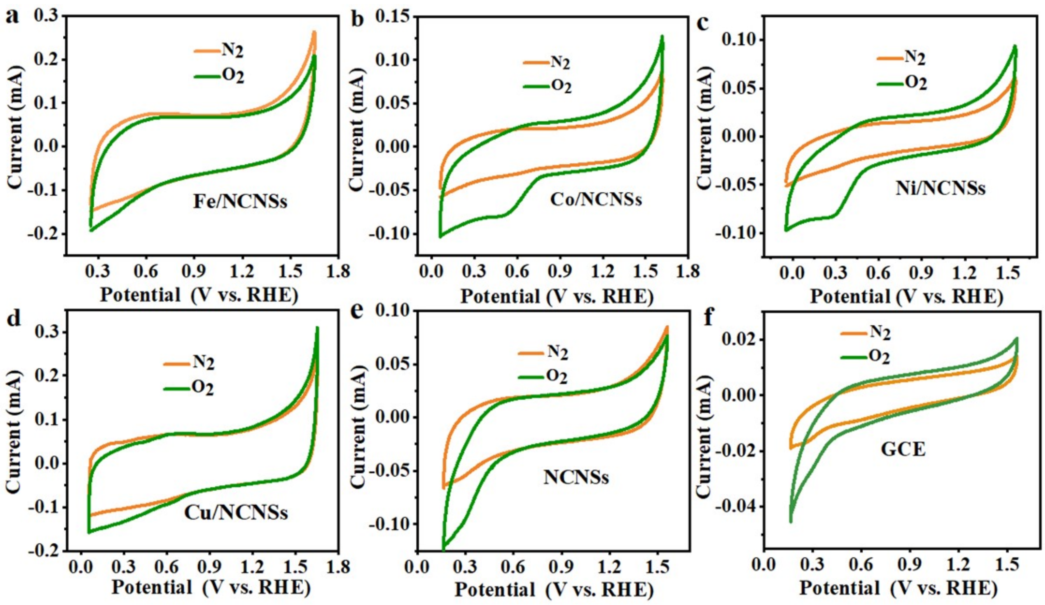

Figure S9 Cyclic voltammetry curves of (a) Fe/NCNSs, (b) Co/NCNSs, (c) Ni/NCNSs, (d) Cu/NCNSs, (e) NCNSs and (f) blank GCE acquired in O_2-saturated and N_2-saturated 0.1 M PBS at a scan rate of 50 mV s^{-1}.

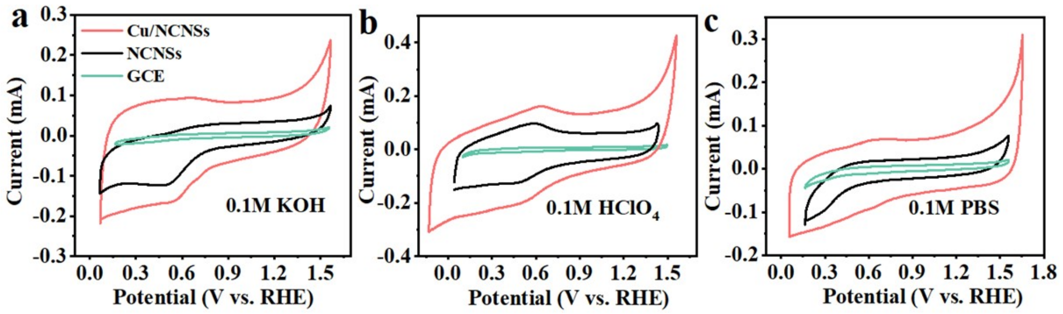

Figure S10 CV curves of Cu/NCNSs, NCNSs and GCE recorded in 0.1 M KOH (a), $HClO_4$ (b) and PBS solutions (c).

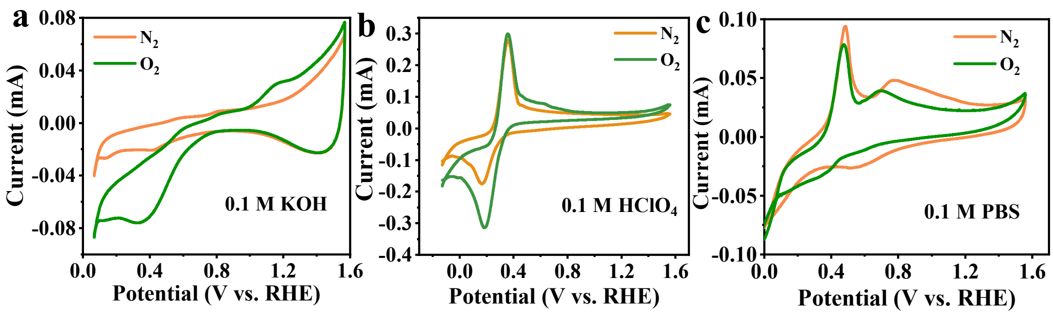

Figure S11 CV curves of Cu NPs recorded in O_2/N_2-saturated 0.1 M KOH (**a**), 0.1 M $HClO_4$ (**b**) and 0.1 M PBS (**c**) solutions.

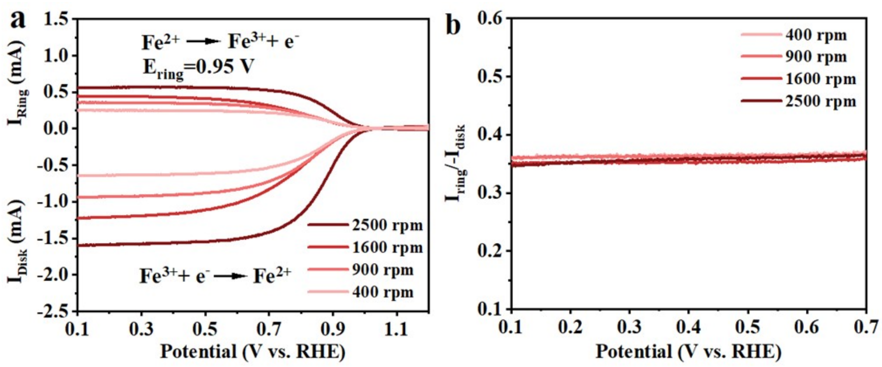

Figure S12 Calibration of the RRDE collection efficiency. (**a**) potentiodynamic curves recorded on the glassy carbon disk electrode and potentiostatic curves recorded on the platinum ring electrode in 1.0 M KCl + 10 mM $K_3[Fe(CN)_6]$ at rotation rates between 400 and 2500 rpm. (**b**) collection efficiency of the RRDE determined by the redox of $K_3[Fe(CN)_6]$.

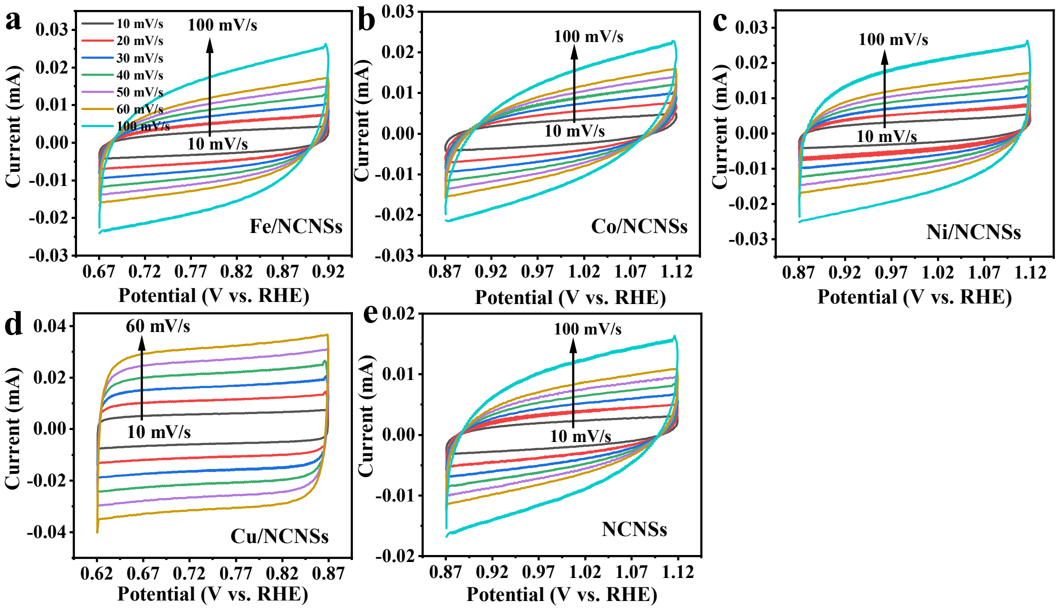

Figure S13 Cyclic voltammetry curves of the Fe/NCNSs (**a**), Co/NCNSs (**b**), Ni/NCNSs (**c**), Cu/NCNSs (**d**) and NCNSs (**e**) recorded with different scan rates in 0.1 M KOH solutions.

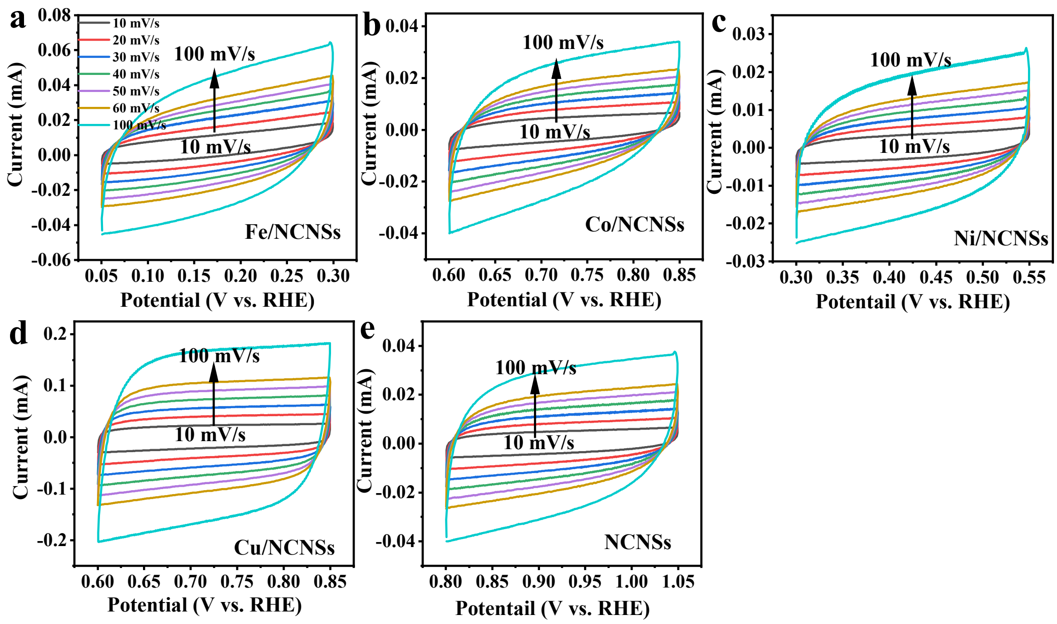

Figure S14 Cyclic voltammetry curves of Fe/NCNSs (**a**), Co/NCNSs (**b**), Ni/NCNSs (**c**), Cu/NCNSs (**d**) and NCNSs (**e**) recorded with different scan rates in 0.1 M $HClO_4$ solutions.

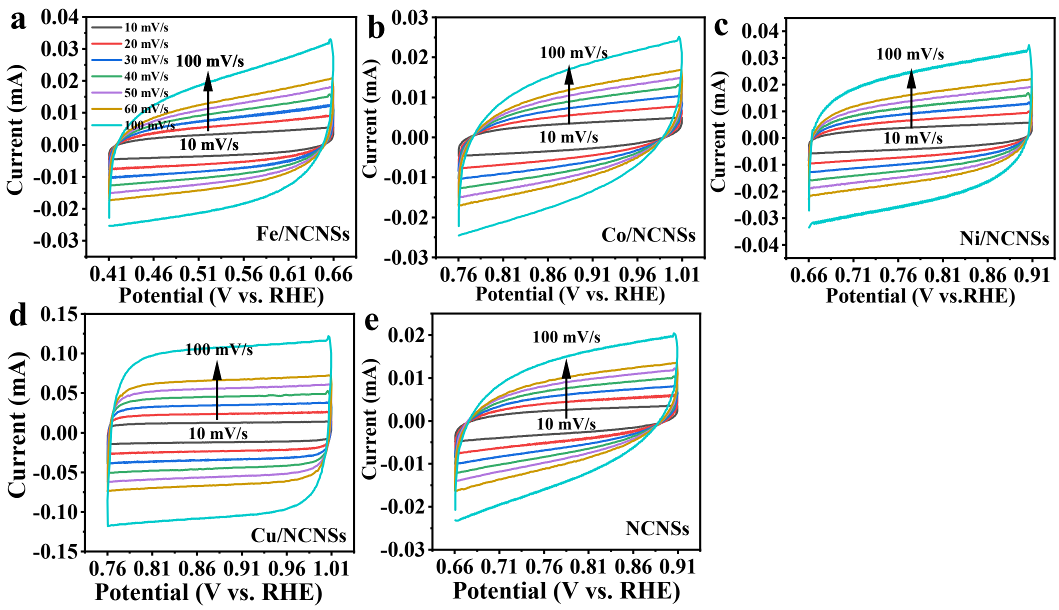

Figure S15 Cyclic voltammetry curves of Fe/NCNSs (**a**), Co/NCNSs (**b**), Ni/NCNSs (**c**), Cu/NCNSs (**d**) and NCNSs (**e**) recorded with different scan rates in 0.1 M PBS solutions.

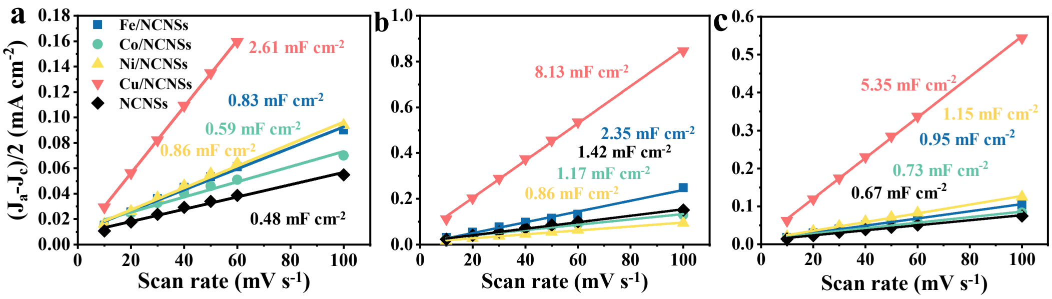

Figure S16 C_{dl} values of the samples in 0.1 M KOH solutions (**a**), 0.1 M $HClO_4$ solutions (**b**) and 0.1 M PBS solutions (**c**).

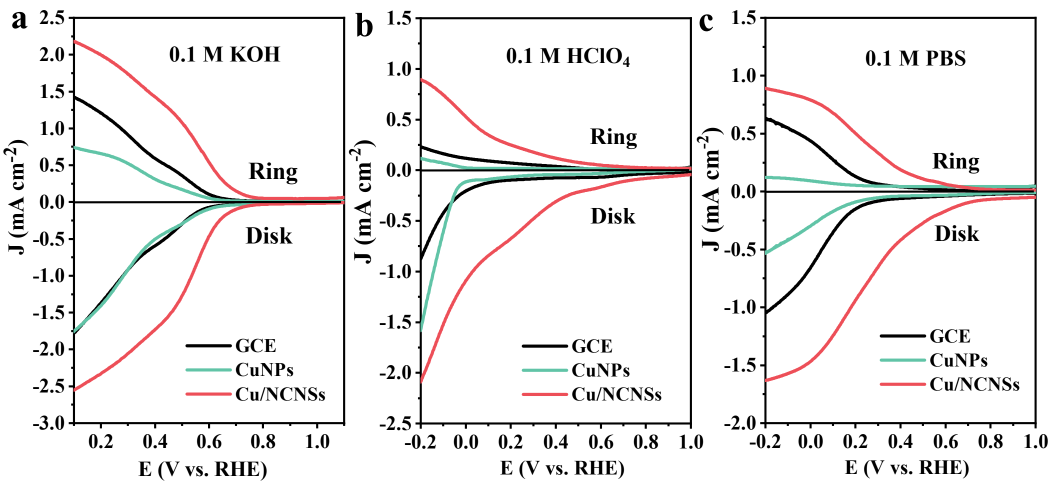

Figure S17 Polarization curves of GCE, Cu NPs and Cu/NCNSs recorded from the RRDE in 0.1 M KOH (**a**), 0.1 M $HClO_4$ (**b**) and 0.1 M PBS (**c**).

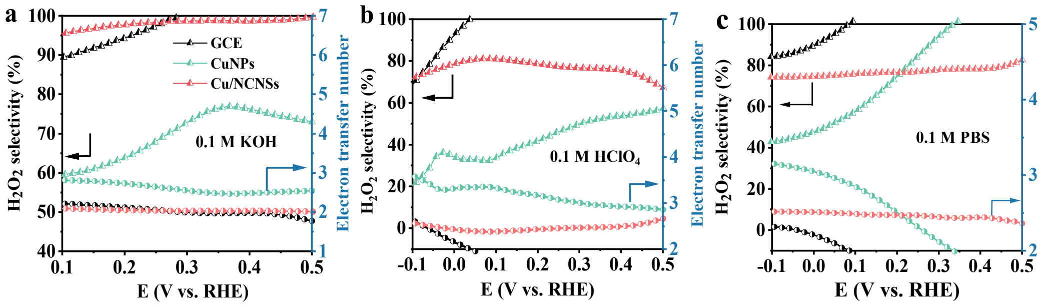

Figure S18 H_2O_2 selectivity and electron transfer number of GCE, Cu NPs and Cu/NCNSs in O_2-saturated 0.1 M KOH (**a**), 0.1 M $HClO_4$ (**b**) and 0.1 M PBS (**c**).

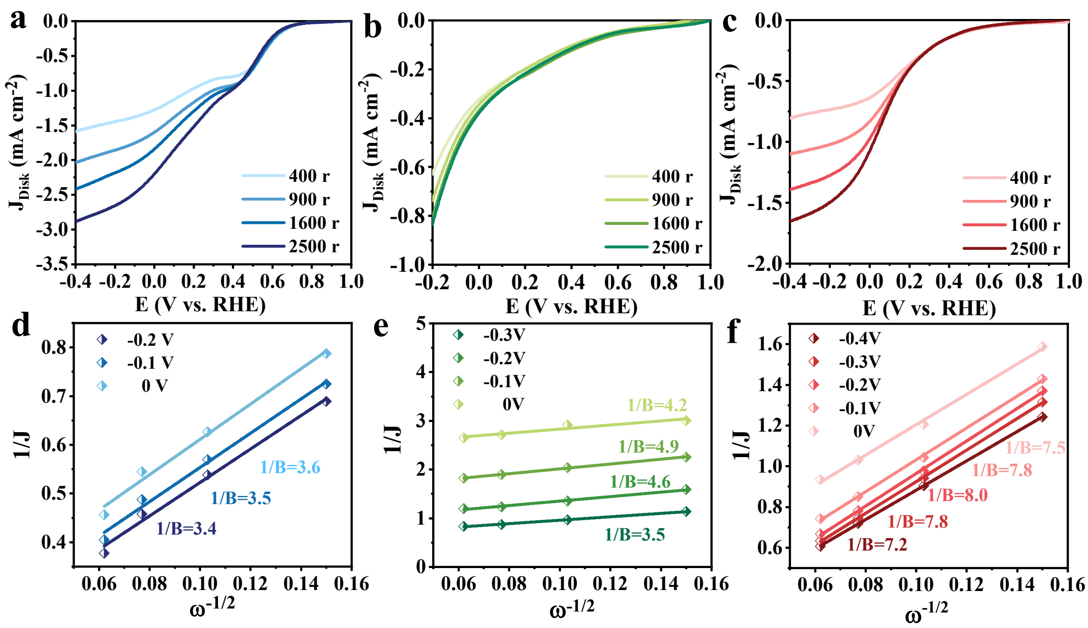

Figure S19 Disk polarization curve of Fe/NCNSs recorded in O_2 saturated 0.1 M KOH (**a**), 0.1 M $HClO_4$ solution (**b**) and 0.1 M PBS (**c**) at different rotation rates between 400 rpm and 2500 rpm, and corresponding K-L plots at different potentials in 0.1 M KOH (**d**), 0.1 M $HClO_4$ (**e**) and 0.1 M PBS (**f**).

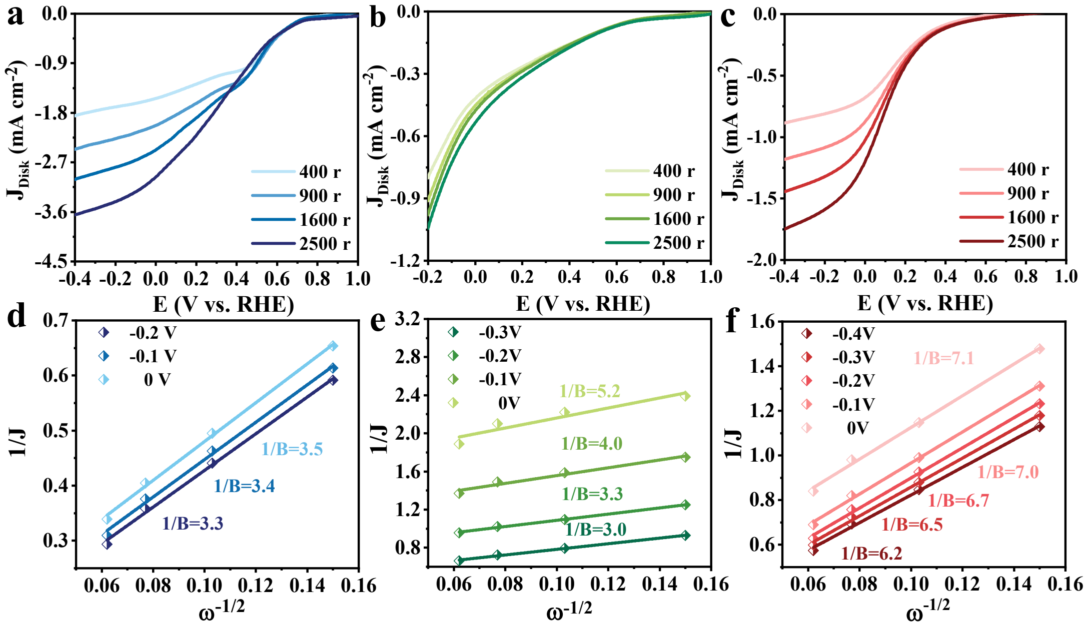

Figure S20 Disk polarization curve of Co/NCNSs recorded in O_2 saturated 0.1 M KOH (**a**), 0.1 M $HClO_4$ solution (**b**) and 0.1 M PBS (**c**) at different rotation rates between 400 rpm and 2500 rpm, and the corresponding K-L plots at different potentials in 0.1 M KOH (**d**), 0.1 M HClO4 (**e**) and 0.1 M PBS (**f**).

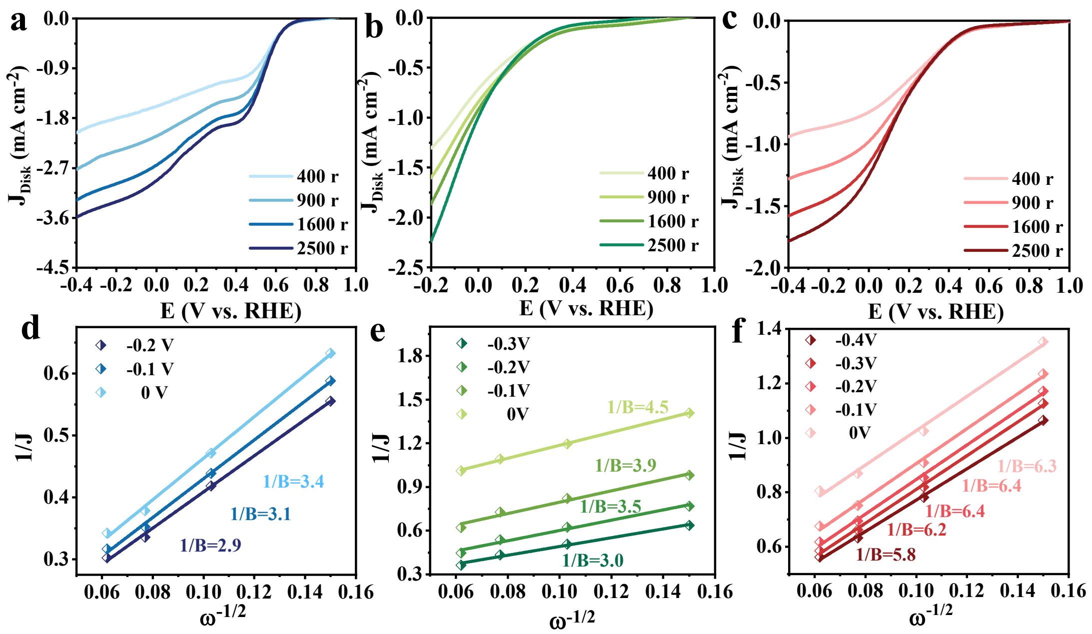

Figure S21 Disk polarization curve of Ni/NCNSs recorded in O_2 saturated 0.1 M KOH (**a**), 0.1 M $HClO_4$ solution (**b**) and 0.1 M PBS (**c**) at different rotation rates between 400 rpm and 2500 rpm, and corresponding K-L plots at different potentials in 0.1 M KOH (**d**), 0.1 M $HClO_4$ (**e**) and 0.1 M PBS (**f**).

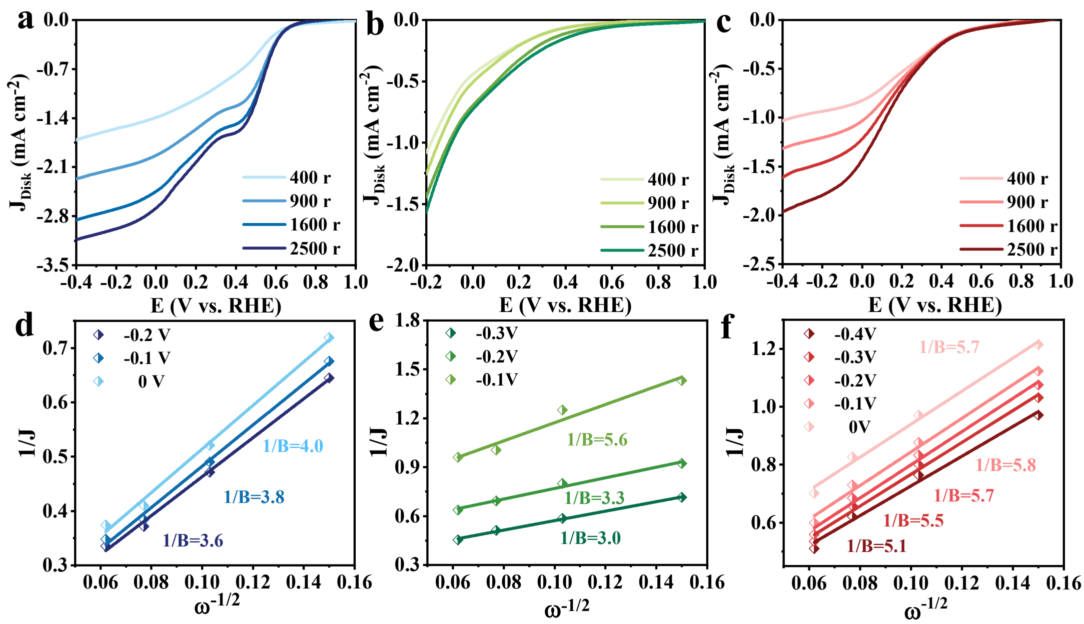

Figure S22 Disk polarization curve of NCNSs recorded in O_2 saturated 0.1 M KOH (**a**), 0.1 M $HClO_4$ solution (**b**) and 0.1 M PBS (**c**) at different rotation rates between 400 rpm and 2500 rpm, and corresponding K-L plots at different potentials in 0.1 M KOH (**d**), 0.1 M $HClO_4$ (**e**) and 0.1 M PBS (**f**).

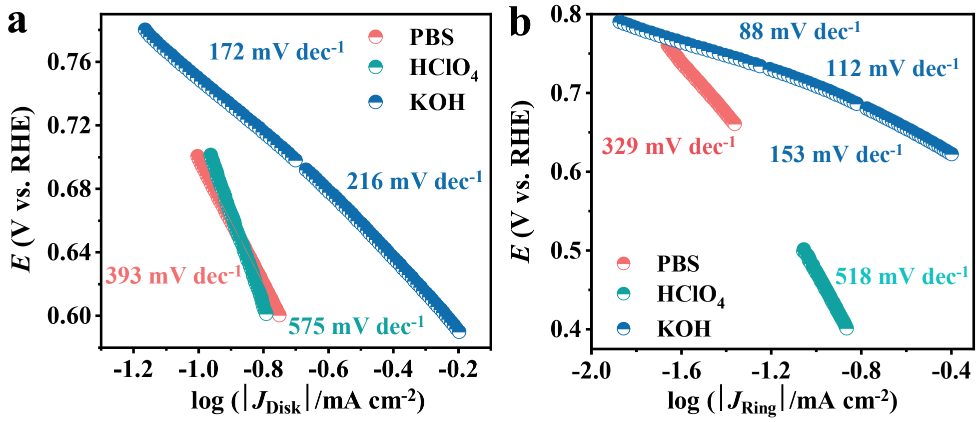

Figure S23 Tafel plots of Cu/NCNSs on the disk (**a**) and ring (**b**) electrodes at a rotating rate of 1600 rpm in the O_2-satureted KOH, $HClO_4$ and PBS media.

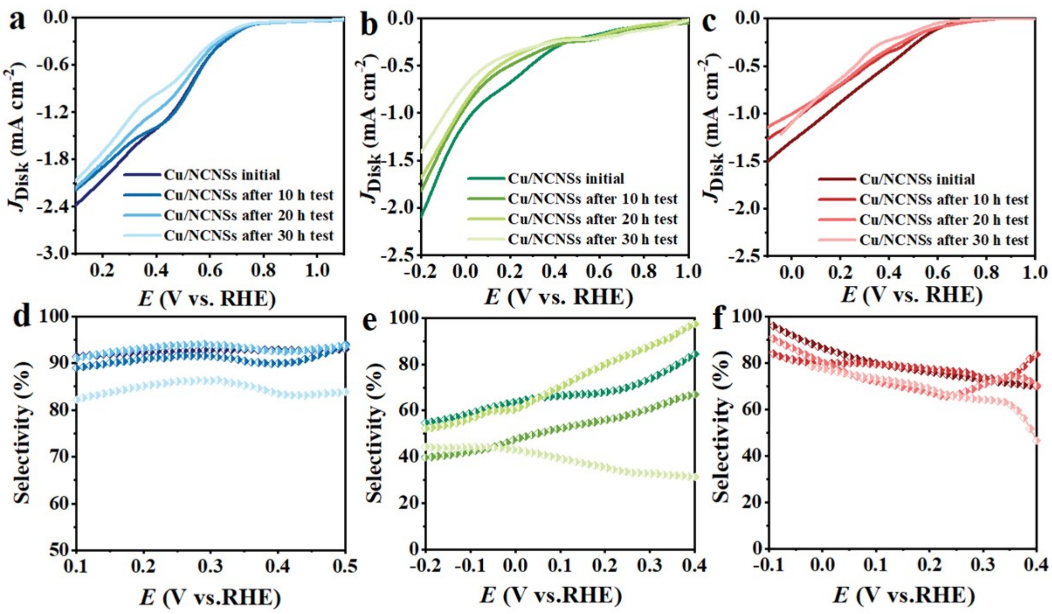

Figure S24 Polarization curve of Cu/NCNSs recorded in 0.1 M KOH (**a**), 0.1 M $HClO_4$ (**b**) and 0.1 M PBS (**c**) solutions, and the corresponding selectivity in 0.1 M KOH (**d**), 0.1 M $HClO_4$ (**e**) and 0.1 M PBS (**f**).

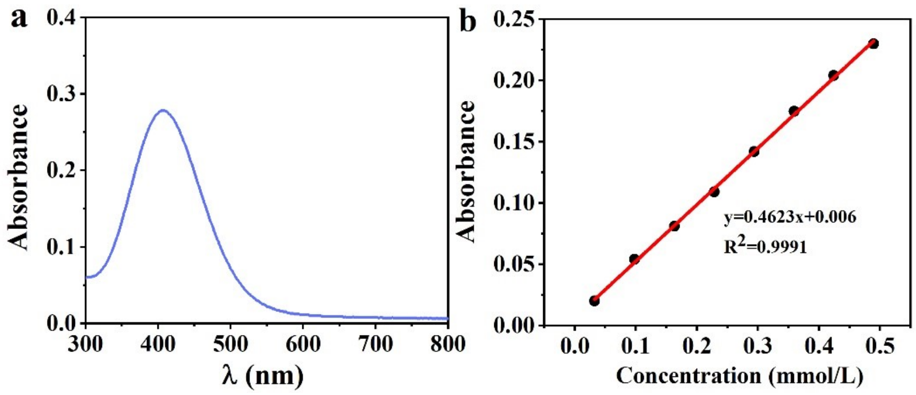

Figure S25 A typical UV curve of H_2O_2 scanning spectrum (**a**), and standard curve of H_2O_2 determined by titanium sulfate spectrophotometric method (**b**).

References

1 D. A. Kuznetsov, Z. Chen, P. M. Abdala, O. V. Safonova, A. Fedorov and C. R. Müller, *J. Am. Chem. Soc.*, 2021, **143**, 5771–5778.

2 H. Xiao, B. Li, M. Zhao, Y. Li, T. Hu, J. Jia and H. Wu, *Chem. Commun.*, 2021, **57**, 4118–4121.

3 Y. Pang, K. Wang, H. Xie, Y. Sun, M.-M. Titirici and G.-L. Chai, *ACS Catal.*, 2020, **10**, 7434–7442.

4 Y. Sun, L. Silvioli, N. R. Sahraie, W. Ju, J. Li, A. Zitolo, S. Li, A. Bagger, L. Arnarson, X. Wang, T. Moeller, D. Bernsmeier, J. Rossmeisl, F. Jaouen and P. Strasser, *J. Am. Chem. Soc.*, 2019, **141**, 12372–12381.

5 E. Chen, M. Bevilacqua, C. Tavagnacco, T. Montini, C.-M. Yang and P. Fornasiero, *Catal. Today*, 2020, **356**, 132–140.

6 M. Wang, X. Dong, Z. Meng, Z. Hu, Y. Lin, C. Peng, H. Wang, C. Pao, S. Ding, Y. Li, Q. Shao and X. Huang, *Angew. Chem. Int. Ed.*, 2021, **60**, 11190–11195.

7 C. Tang, Y. Jiao, B. Shi, J. Liu, Z. Xie, X. Chen, Q. Zhang and S. Qiao, *Angew. Chem. Int. Ed.*, 2020, **59**, 9171–9176.

8 B. Li, C. Zhao, J. Liu and Q. Zhang, *Adv. Mater.*, 2019, **31**, 1808173.

9 C. H. Choi, W. S. Choi, O. Kasian, A. K. Mechler, M. T. Sougrati, S. Brüller, K. Strickland, Q. Jia, S. Mukerjee, K. J. J. Mayrhofer and F. Jaouen, *Angew. Chem. Int. Ed.*, 2017, **56**, 8809–8812.

10 V. Perazzolo, C. Durante, R. Pilot, A. Paduano, J. Zheng, G. A. Rizzi, A. Martucci, G. Granozzi and A. Gennaro, *Carbon*, 2015, **95**, 949–963.

11 S. Chen, Z. Chen, S. Siahrostami, T. R. Kim, D. Nordlund, D. Sokaras, S. Nowak, J. W. F. To, D. Higgins, R. Sinclair, J. K. Nørskov, T. F. Jaramillo and Z. Bao, *ACS Sustainable Chem. Eng.*, 2018, **6**, 311–317.

12 A. Moraes, M. H. M. T. Assumpção, F. C. Simões, V. S. Antonin, M. R. V. Lanza, P. Hammer and M. C. Santos, *Electrocatalysis*, 2016, **7**, 60–69.

13 Z. Lu, G. Chen, S. Siahrostami, Z. Chen, K. Liu, J. Xie, L. Liao, T. Wu, D. Lin, Y. Liu, T. F. Jaramillo, J. K. Nørskov and Y. Cui, *Nat. Catal.*, 2018, **1**, 156–162.

14 S. Chen, Z. Chen, S. Siahrostami, D. Higgins, D. Nordlund, D. Sokaras, T. R. Kim, Y. Liu, X. Yan, E. Nilsson, R. Sinclair, J. K. Nørskov, T. F. Jaramillo and Z. Bao, *J. Am. Chem. Soc.*, 2018, **140**, 7851–7859.

15 X. Yang, Y. Zeng, W. Alnoush, Y. Hou, D. Higgins and G. Wu, *Adv. Mater.*, 2022, **34**, 2107954.

16 J. Zhang, J. Ma, T. S. Choksi, D. Zhou, S. Han, Y.-F. Liao, H. B. Yang, D. Liu, Z. Zeng, W. Liu, X. Sun, T. Zhang and B. Liu, *J. Am. Chem. Soc.*, 2022, **144**, 2255–2263.

17 E. Zhang, L. Tao, J. An, J. Zhang, L. Meng, X. Zheng, Y. Wang, N. Li, S. Du, J. Zhang, D. Wang and Y. Li, *Angew. Chem. Int. Ed*., 2022, **61**, e202117347.

18 C. Liu, H. Li, F. Liu, J. Chen, Z. Yu, Z. Yuan, C. Wang, H. Zheng, G. Henkelman, L. Wei and Y. Chen, *J. Am. Chem. Soc.*, 2020, **142**, 21861–21871.

19 C.-Y. Chen, C. Tang, H.-F. Wang, C.-M. Chen, X. Zhang, X. Huang and Q. Zhang, *ChemSusChem*, 2016, **9**, 1194–1199.

20 S. Siahrostami, A. Verdaguer-Casadevall, M. Karamad, D. Deiana, P. Malacrida, B. Wickman, M. Escudero-Escribano, E. A. Paoli, R. Frydendal, T. W. Hansen, I. Chorkendorff, I. E. L. Stephens and J. Rossmeisl, *Nat. Mater.*, 2013, **12**, 1137–1143.

21 X. Zhao, Y. Wang, Y. Da, X. Wang, T. Wang, M. Xu, X. He, W. Zhou, Y. Li, J. N. Coleman

and Y. Li, *Natl. Sci. Rev.*, 2020, **7**, 1360–1366.
22 E. Jung, H. Shin, B.-H. Lee, V. Efremov, S. Lee, H. S. Lee, J. Kim, W. Hooch Antink, S. Park, K.-S. Lee, S.-P. Cho, J. S. Yoo, Y.-E. Sung and T. Hyeon, *Nat. Mater.*, 2020, **19**, 436–442.
23 S. Mehta, D. Gupta and T. C. Nagaiah, *ChemElectroChem*, 2022, **9**, e202101336.
24 P. T. Smith, Y. Kim, B. P. Benke, K. Kim and C. J. Chang, *Angew. Chem. Int. Ed.*, 2020, **59**, 4902–4907.
25 N. Wang, X. Zhao, R. Zhang, S. Yu, Z. H. Levell, C. Wang, S. Ma, P. Zou, L. Han, J. Qin, L. Ma, Y. Liu and H. L. Xin, *ACS Catal.*, 2022, **12**, 4156–4164.